Supplementary Information

High Performance Flexible Triboelectric Nanogenerators using Bio-derived Films made of Siloxane-Modified Castor Oil

Kishore K. Jena [1,2†], Bushara Fatma [3†], Sagar S. Arya [1†], Saeed M. Alhassan [2], Vincent Chan [1, 4], Anna Maria Pappa [1,4], Charalampos Pitsalidis [3,4*]

[1] Department of Biomedical Engineering, Khalifa University, PO Box – 127788, Abu Dhabi, United Arab Emirates (UAE)
[2] Department of Chemical Engineering, Khalifa University, PO Box – 127788, Abu Dhabi, United Arab Emirates (UAE)
[3] Department of Physics, Khalifa University, PO Box – 127788, Abu Dhabi, United Arab Emirates (UAE)
[4] Healthcare Engineering Innovation Center (HEIC), Khalifa University of Science and Technology, PO Box – 127788, Abu Dhabi, United Arab Emirates (UAE)
*Correspondence: charalampos.pitsalidis@ku.ac.ae (CP)

†Contributed equally

S1.1. Characterization techniques

The structure of all materials used in reaction for synthesis of hybrid films were characterized by FTIR spectroscopy on a Bruker Vertex 70 V using ATR method. Each sample was scanned within the range 400-4000 cm $^{-1}$. Thermogravimetric analysis (TGA) was conducted from room temperature to 700 °C using a NETZSCH High-Temperature TGA (USA) thermal analyser at a heating rate of 10 °C min^{-1} under nitrogen atmosphere. The mechanical properties of the prepared film were tested using an Instron 2519-107 universal testing machine (InstronCorp.). ASTM standard test method D 6382 was adopted, and the straining rate was kept at 5 mm per min. The uniform films were cut into standard length and width strips and the testing was conducted at room temperature using plain rubber grips. The atomic force microscopic (AFM) technique was used to study the surface morphology of the castor oil-amine-TMSPM-VTES UV-cured hybrid samples. The solutions of the castor oil-amine-TMSPM-VTES samples coated on the top of polished aluminum surface and then hardened by using

UV curing process. The Bruker Multimode 8 operating in ScanAsyst mode was used to capture the surface topography. The 3D images were created using TrueMap software from TrueGage Surface Metrology. Contact angle measurements were done to determine the hydrophilic and hydrophobic nature of the hybrid films using contact angle measuring instrument goniometer, at ambient temperatures. The volume of the water droplets was 1μL and the contact angle was measured 10 different places of the hybrid film samples. The contact angles were evaluated using sensible drop method which involves placing a drop of water using a micro syringe on the dry films and then measuring the contact angle between the solid-liquid interfaces. Morphological characterization for the films and the bacterial studies was performed using SEM, JEOL JSM-7610F Field Emission Gun (Tokyo, Japan). The films were coated with gold for 11 seconds at a 5 kV acceleration voltage. Micrographs were taken at 5 kV, 1-KX magnifications, and a working distance of 8.0 m to reveal the surface of the films. Additionally, Kelvin probe force microscopy (KPFM) used to obtain the surface potential of the CO-based films in scan area of 5x5 um (Asylum Research, Model: MFP-3D).

Scheme S1. Reaction steps involved during castor oil-amine-TMSPM (COAmT) synthesis.

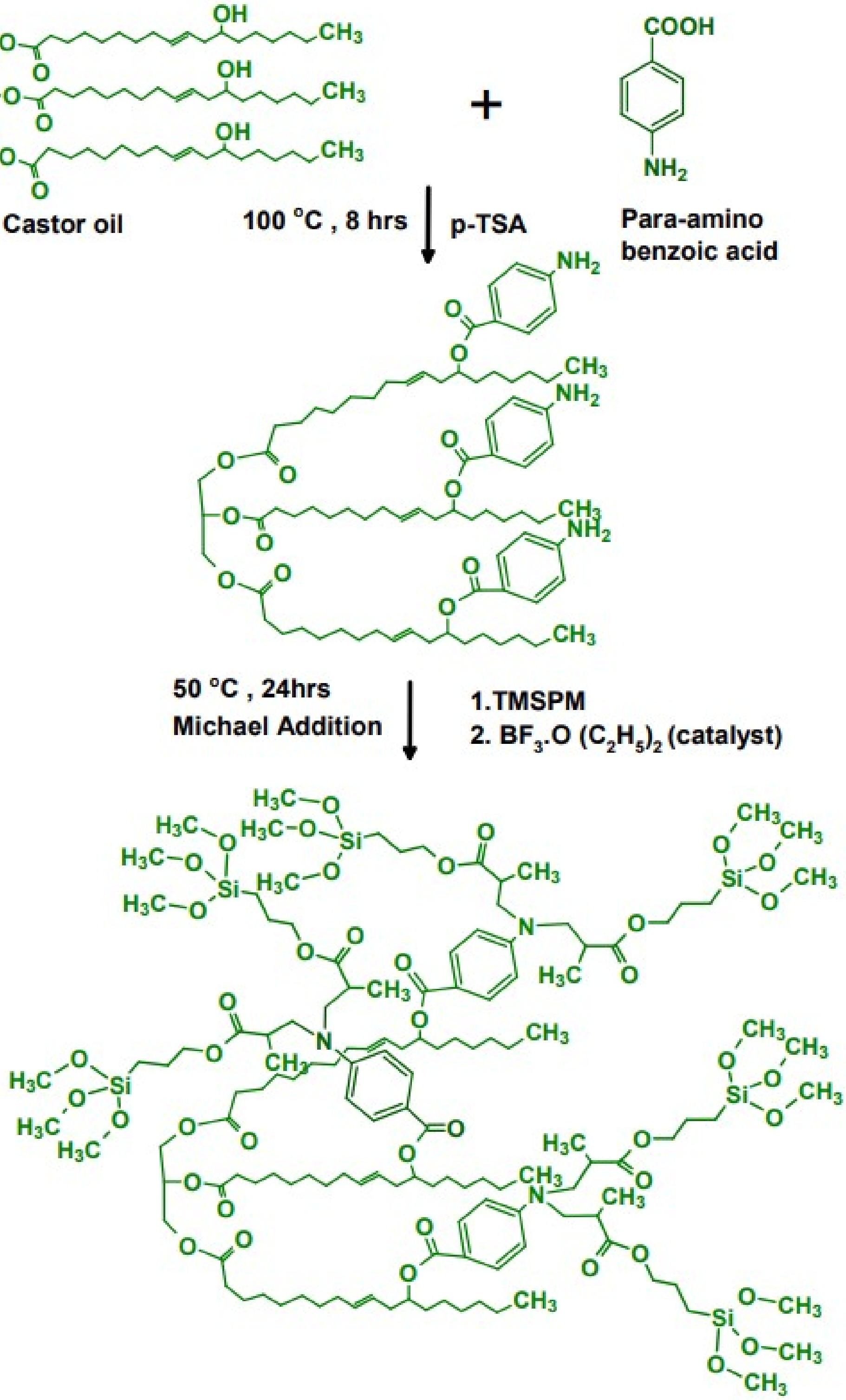

Scheme S2. Synthetic route for the development of Castor oil-amine-TMSPM-VTES (COAmTMS-VT) hybrid. ***Reaction A:*** Castor oil-amine-TMSPM-VTES reaction steps and ***Reaction B:*** UV curing reaction step showing how polymerization occurs in the hybrid system during the solgel-gel and UV curing process.

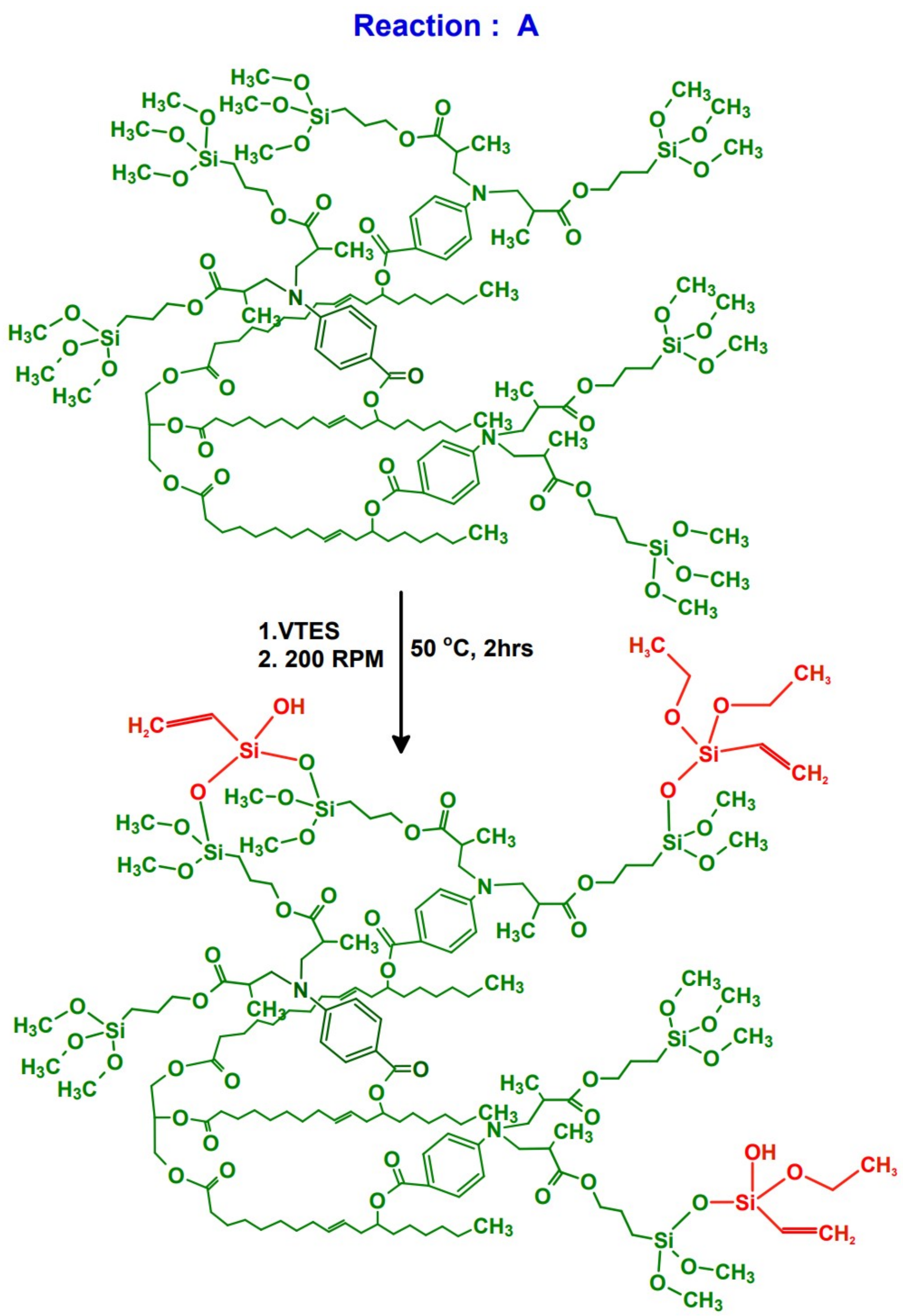

Reaction :B

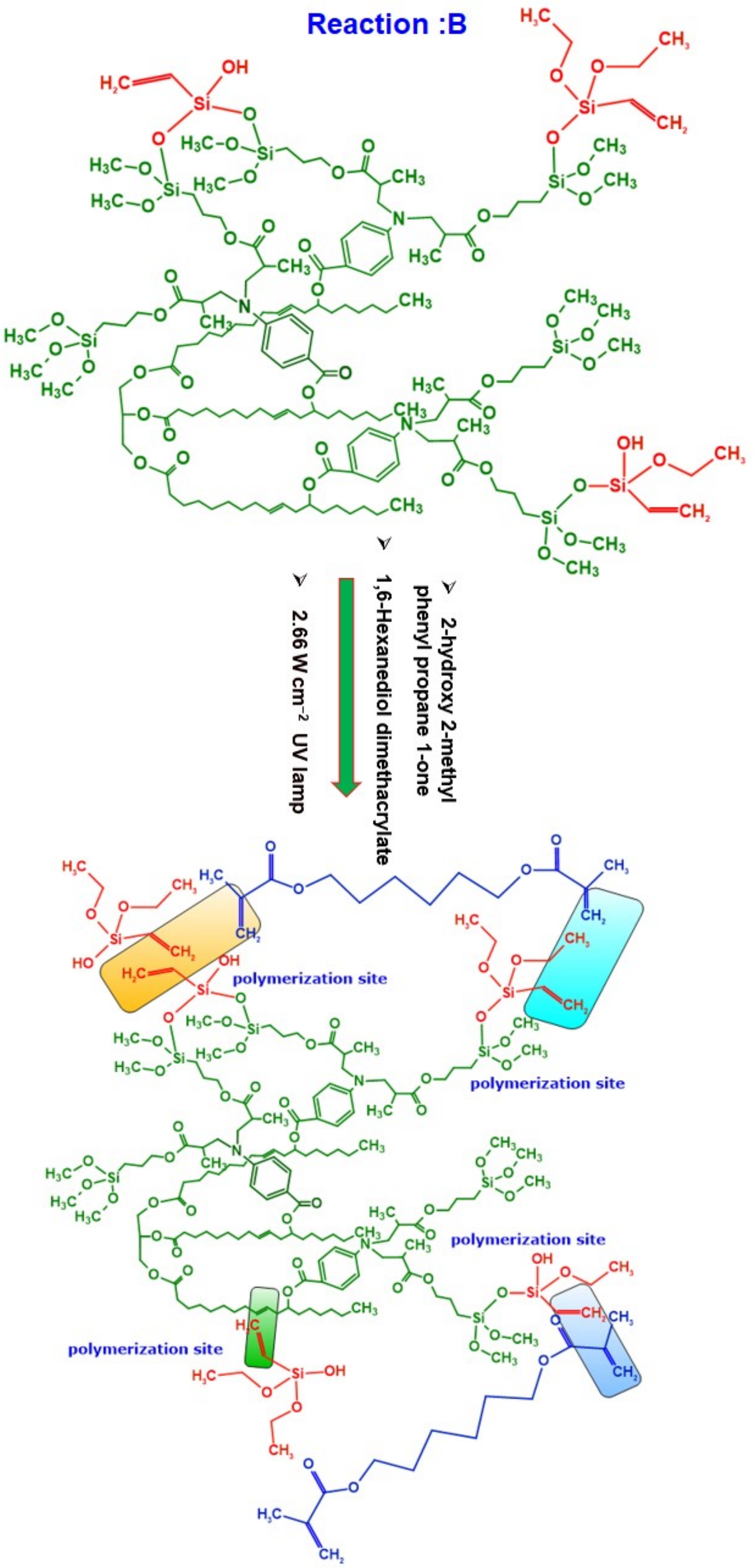
2-hydroxy 2-methyl phenyl propane 1-one
1,6-Hexanediol dimethacrylate
2.66 W cm^{-2} UV lamp
polymerization site
polymerization site
polymerization site
polymerization site

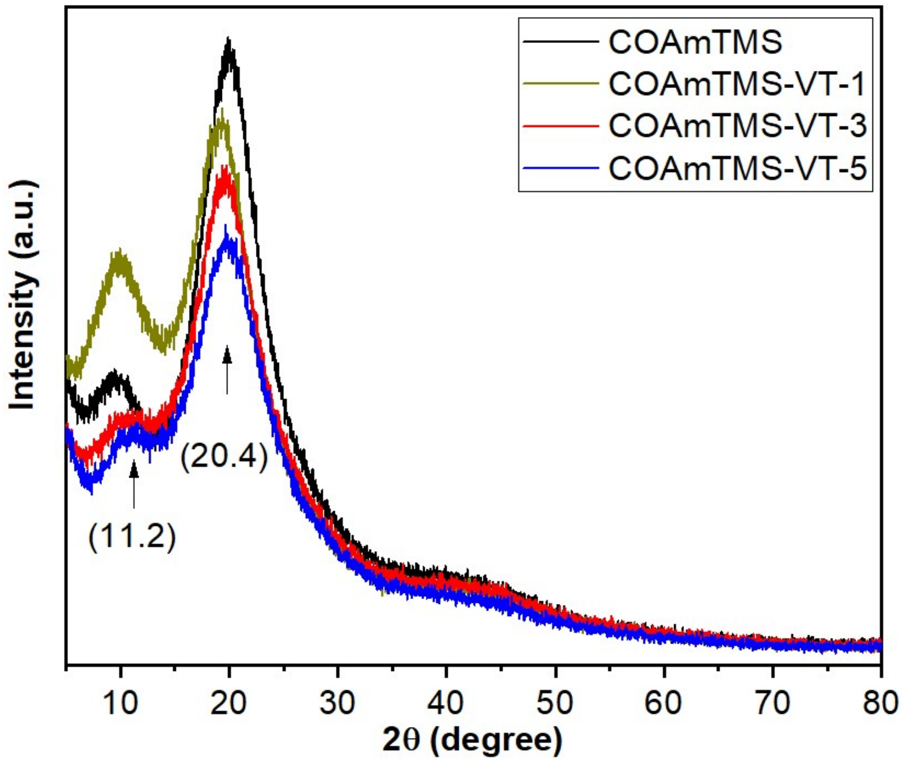

Figure S1. XRD spectra of COAmTMS, COAmTMS-VT-1, COAmTMS-VT-3, and COAmTMS-VT-5 materials.

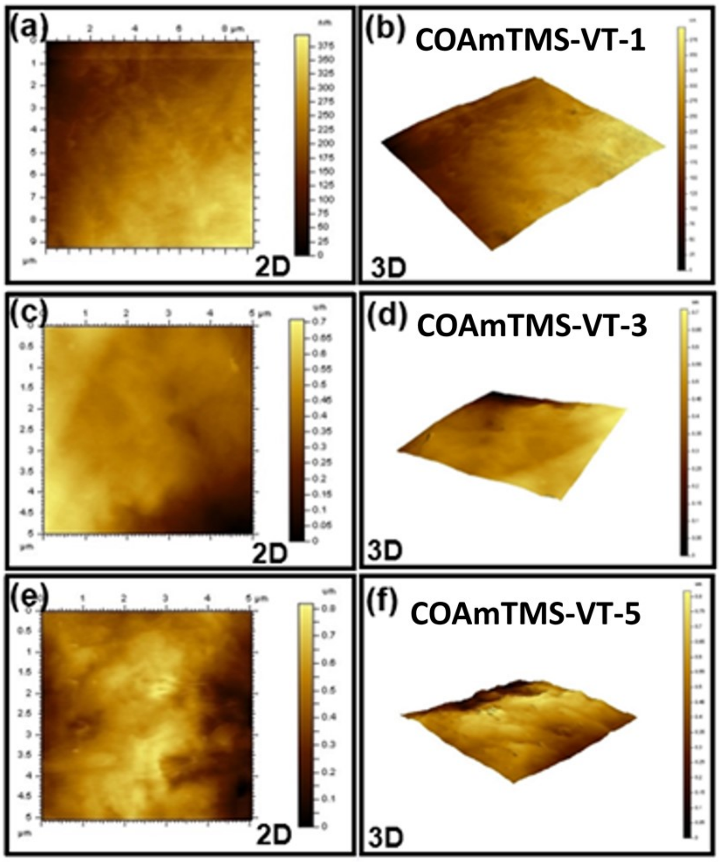

Figure S2 (a-f). 2D and 3D AFM images of COAmTMS-VT-1, COAmTMS-VT-3 and COAmTMS-VT-5.

Table S1. Surface Roughness and water contact angle data of COAmTMS, COAmTMS-VT-1 COAmTMS-VT-3 and COAmTMS-VT-5 hybrid samples.

Sample Code	Roughness (RMS) (nm)	Water Contact angle (°)
COAmTMS-VT-1	5.7	86 ± 5.3
COAmTMS-VT-3	6.9	91 ± 2.5
COAmTMS-VT-5	7.4	101 ±1.6

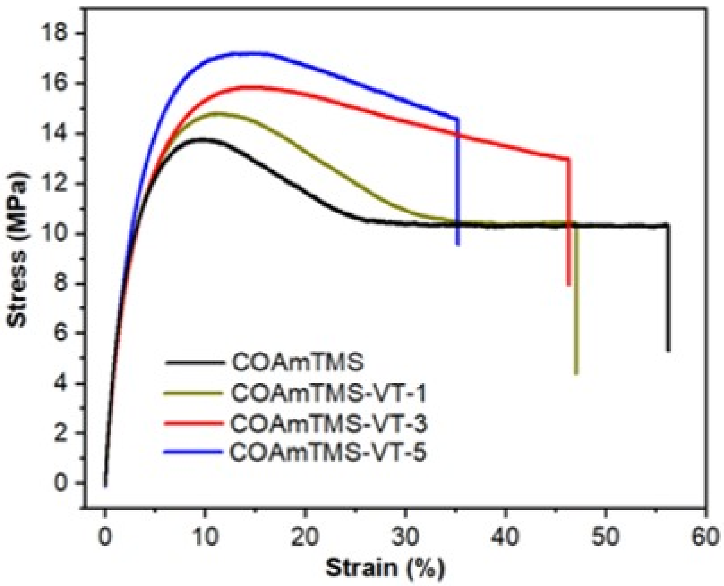

Figure S3. Stress-strain curve of COAmTMS, COAmTMS-VT-1, COAmTMS-VT-3 and COAmTMS-VT-5 samples.

Table S2: UTM data of the COAmTMS, COAmTMS-VT-1, COAmTMS-VT-3 and COAmTMS-VT-5 films.

Sample Name	Ultimate tensile strength (MPa)	Elongation (%)	Modulus (MPa)
COAmTMS	12.9 ±1.1	57.6 ±4.8	377.2 ±12.4
COAmTMS-VT-1	14.4 ±2.5	46.2 ±3.6	388.1 ± 13.9
COAmTMS-VT-3	15.6 ±1.9	45.6 ±3.2	411.7±16.4
COAmTMS-VT-5	17.5 ±3.1	35.2 ±2.9	461.1±18.2

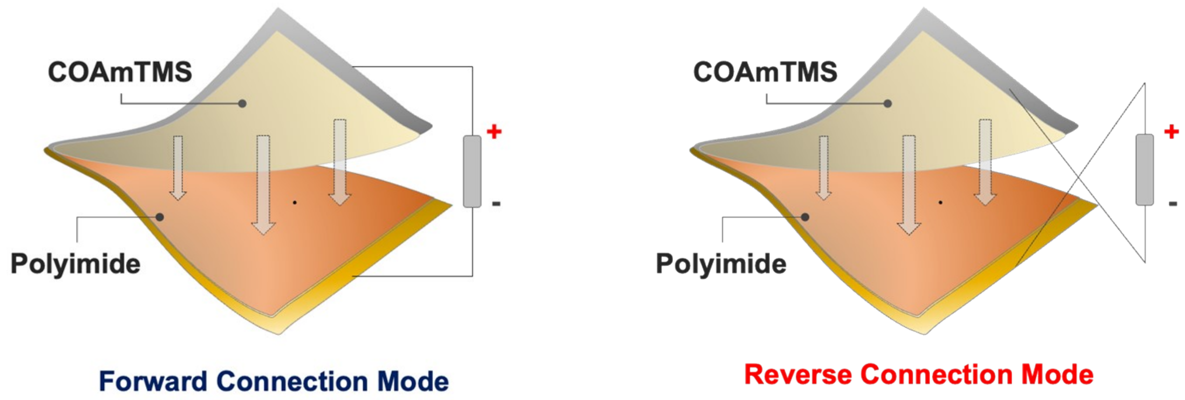

Figure S4. Illustrations of the (a) forward mode and (b) reverse mode connections which are utilized to obviate any potential system anomalies.

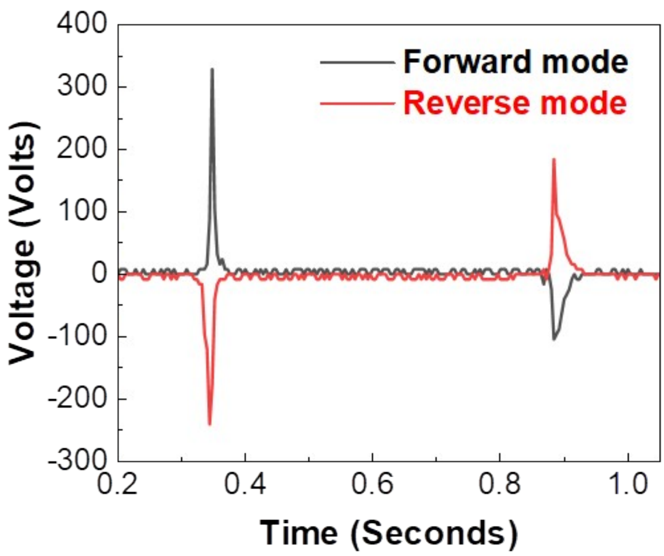

Figure S5. TENG's voltage response for a single press-and-release cycle in forward and reverse mode connections. Generated outputs are similar and reverse in nature, indicating that it is a legitimate TENG signal.

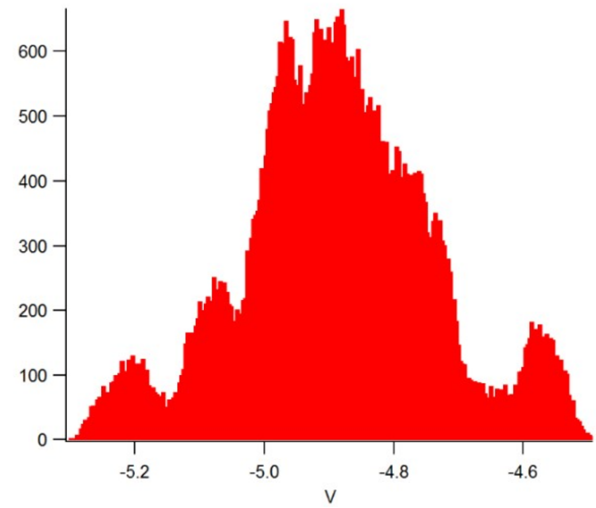

Figure S6. Histogram showing the surface potential distribution of COAmTMS film based on its KPFM study.

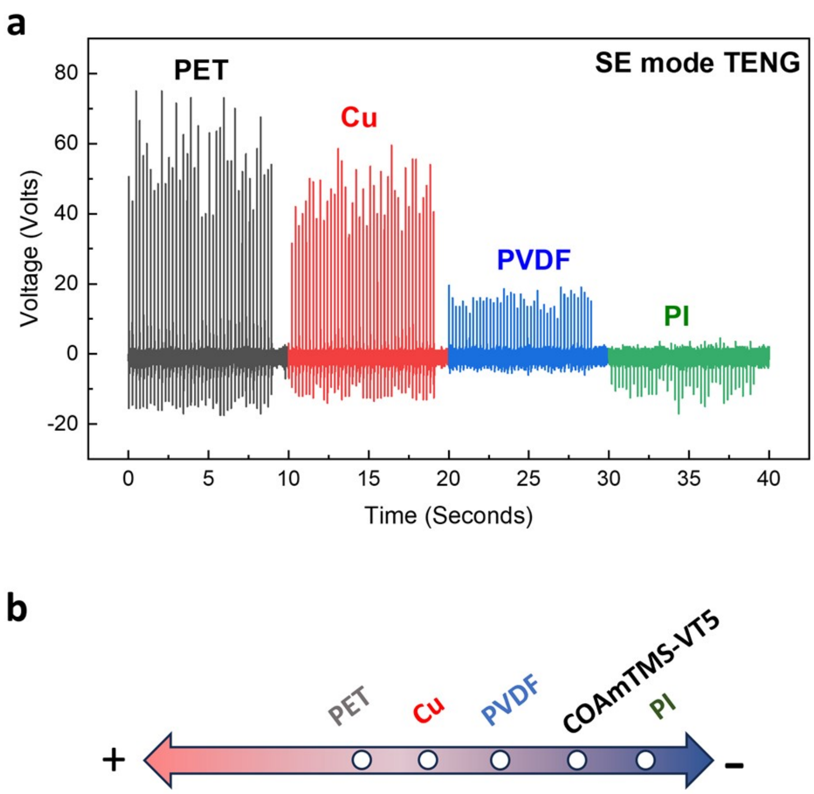

Figure S7. (a) Output voltage of COAmTMS-VT-5 TENG in single electrode (SE-TENG) mode via contact-separation motion using electrically free triboelectric layer of polyethylene terthalate (PET), copper (Cu), polyvinylidene fluoride (PVDF) or polyimide (PI). (b) Triboelectric series for the different friction layers derived from the performance output of the SE-TENG.

Table S3. Comparison of our CO-based TENG devices with other biopolymer based TENGsreported in literature.

#	Triboelectric Material	Nature of triboelectric layers	Polarity of biopolymer	Electrode Material	Mode of Operation	Voltage (V) / Power density (mW/m^2)	Ref
1.	Polyamide made of soybean oil/PTFE	All-biopolymer	Positive	Cu	SE	~150/---	**[1]**
2.	Cellulose nanofibrils (CNF), FEP	Biopolymer vs synthetic polymer	Positive	ITO	CS	~30/ ~6mW	**[2]**
3.	Paper, FEP (Hybrid)	Biopolymer vs synthetic polymer	Positive	ITO	CS/ SE	~90/ ~300	**[3]**
4.	PDMS, cellulose nanofiber aerogel	Biopolymer vs synthetic polymer	Positive	Ag	CS	~50	**[4]**
5.	CNF, FEP	Biopolymer vs synthetic polymer	Positive	Cu	CS	~76/ ---	**[5]**
6.	Polypyrrole coated cotton/PDMS	Biopolymer vs synthetic polymer	Positive	ITO, Ag	CS	~200/ 900	**[6]**
7.	Paper, PVC, PET	Biopolymer vs synthetic polymer	Positive	Paper+ Ag nanowire	FS	~100	**[7]**
8.	Bacterial nanocellulose, Cu	All-biopolymer	Positive	Cu	CS	~13/4.4	**[8]**
9.	Egg white, chitin, cellulose, raw silk, rice paper	All-biopolymer	Positive/ negative	Mg	CS	~50	**[9]**
10.	Cellulose, Cellulose+Ag	All-biopolymer	Positive	Ag nanowire	CS	~21/693	**[10]**
11.	PLGA, PHB/V, PVA, PCL	All-biopolymer	Positive/ negative	Mg	CS	40/32.6	**[11]**
12.	BC, PPBC,PDBC, SBC, PVDF	Biopolymer vs synthetic polymer	Positive	Cu	CS	~1010/ 8700	**[12]**
	BC, PPBC, PDBC, SBC	All-biopolymer	Positive/ negative	Cu	CS	~42.7/9.2	
	PDBC	All-biopolymer	Positive	MWCNT/ BC	SE	~200	

13.	COAmTMS/PI	Biopolymer vs synthetic polymer	Negative	Cu, Al	CS	~330/450	
	COAmTMS/COAmTMS-VT-5	All-biopolymer	Positive/negative	Cu, Al	CS	~55/18	**This work**
	COAmTMS-VT-5	All-biopolymer	Negative	Al	SE	~75	

*CS – *Contact separation,* SE – *Single electrode,* FS – *Free standing.*

References:

1. W. Intarabumrung, S. Kuntharin, V. Harnchana, T. Prada, P. Kasemsiri, A. J. Hunt and N. Supanchaiyamat, *ACS Sustainable Chemistry & Engineering*, 2022, **10**, 13680-13691.
2. C. Yao, A. Hernandez, Y. Yu, Z. Cai and X. Wang, *Nano Energy*, 2016, **30**, 103-108.
3. X. He, Y. Zi, H. Yu, S. L. Zhang, J. Wang, W. Ding, H. Zou, W. Zhang, C. Lu and Z. L. Wang, *Nano Energy*, 2017, **39**, 328-336.
4. C. Qian, L. Li, M. Gao, H. Yang, Z. Cai, B. Chen, Z. Xiang, Z. Zhang and Y. Song, *Nano Energy*, 2019, **63**, 103885.
5. Y. Liu, Q. Fu, J. Mo, Y. Lu, C. Cai, B. Luo and S. Nie, *Nano Energy*, 2021, **89**, 106369.
6. A. R. Mule, B. Dudem, H. Patnam, S. A. Graham and J. S. Yu, *ACS Sustainable Chemistry & Engineering*, 2019, **7**, 16450-16458.
7. C. Wu, T. W. Kima, S. Sung, J. H. Park and F. Li, *Nano Energy*, 2018, **44**, 279-287.
8. H.-J. Kim, E.-C. Yim, J.-H. Kim, S.-J. Kim, J.-Y. Park and I.-K. Oh, *Nano Energy*, 2017, **33**, 130-137.
9. W. Jiang, H. Li, Z. Liu, Z. Li, J. Tian, B. Shi, Y. Zou, H. Ouyang, C. Zhao, L. Zhao, R. Sun, H. Zheng, Y. Fan, Z. L. Wang and Z. Li, *Advanced Materials*, 2018, **30**, 1801895.
10. I. Kim, H. Jeon, D. Kim, J. You and D. Kim, *Nano Energy*, 2018, **53**, 975-981.
11. Q. Zheng, Y. Zou, Y. Zhang, Z. Liu, B. Shi, X. Wang, Y. Jin, H. Ouyang, Z. Li and Z. L. Wang, *Science Advances*, **2**, e1501478.
12. B. Fatma, S. M. Andrabi, S. Gupta, V. Verma, A. Kumar, C. Pitsalidis and A. Garg, *Nano Energy*, 2023, **114**, 108628.